5-1-2005

Electronic structure of sulfur-modified nanocrystalline carbon films

S. Gupta
Missouri State University

B. R. Weiner

G. Morell

Recommended Citation

Gupta, S., B. R. Weiner, and G. Morell. "Electronic structure of sulfur-modified nanocrystalline carbon films." Journal of applied physics 97, no. 9 (2005): 094307.

Electronic structure of sulfur-modified nanocrystalline carbon films

S. Gupta[a)]
Department of Physics, Astronomy, and Materials Science, Southwest Missouri State University, Springfield Missouri 65804-0027

B. R. Weiner and G. Morell
Department of Chemistry and Physical Sciences, University of Puerto Rico, San Juan, P.O. Box 23323, Puerto Rico 00931-3323

(Received 15 November 2004; accepted 18 February 2005; published online 20 April 2005)

Thin films of nanocrystalline diamond were grown by filament-assisted chemical-vapor deposition using methane as carbon precursor with high hydrogen dilution and hydrogen sulfide concentration ranging from 0 to 500 ppm in the gas phase. The surface topography and electronic structure of these films (*n*-C:S) were investigated using ultrahigh-vacuum scanning tunneling microscopy and scanning tunneling spectroscopy (STS), respectively. Topographic image analyses depict that the root-mean-square roughness of the film surface and average grain size decreases with increasing sulfur incorporation either in gas phase or solid films. High-resolution scanning tunneling microscopy images reveal the localized regions of high conductivity (*white*) surrounded by less conductive regions (*black*) pointing at the existence of inhomogeneous mixture of sp^2- and sp^3-bonded carbon in aggregate or clustered and dispersed state. The surface density of states was determined using scanning tunneling spectroscopy where normalized differential conductivity, i.e., $(dI/dV)/(I/V)$ mimics local density of states (DOS). These methods were employed to understand the role of sulfur in the modification of both the surface microstructure and electronic structure near the Fermi level. The band edges were derived by taking tangents to the differential conductivity (dI/dV) within a certain potential window of ±2 eV of the Fermi level. The resulting band gap is found to be similar to that measured optically (Tauc gap). The Fermi level for undoped nanocrystalline carbon (*n*-C) was found just below the midgap indicating that *n*-C is a weakly *p*-type semiconductor. The STS DOS shows oscillatory behavior or peaks which we ascribe to states of the surface layer having relatively more graphitic or sp^2-bonded carbon bonds. With higher sulfur addition, the Fermi level is found to move above the midgap. These results seem to agree quite well with our early work on electrical conductivity exhibiting *n*-type doping taking place and declining band gap at higher sulfur contents measured with spectroscopic ellipsometry technique on the same samples. © *2005 American Institute of Physics*. [DOI: 10.1063/1.1888025]

I. INTRODUCTION

Diamond thin films grown by chemical-vapor deposition (CVD) techniques possess enormous potential and interest and its usage has been persisted for more than a decade in technological arena such as hard coatings, optical windows, surface acoustic wave (SAW) devices, electrochemical electrodes, conformal coating for micro-electromechanical systems (MEMs), and electron emitting surfaces for field-emission displays (FEDs). Each of these applications requires that diamond properties be optimized to fulfill different functionalities including hardness, surface smoothness, optical transparency, electrical conductivity, field emission, and so on, which are usually achieved by operating only on the microstructure. By continuous reduction in crystallite size, the physical properties (mechanical, electrical, and electronic properties) of the resulting material were enhanced substantially.[1–3] For instance, going from an insulating to an electrically conducting (i.e., semiconducting to metallic) material is largely due to the enhancement of grain boundaries (GBs), which is primarily π bonded. In fact, since the number of grain boundaries increases vastly, the entire film becomes electrically conducting and enables it as an excellent cold cathode material while opening new possibilities for probing the structure of matter at the atomic level.[4] Indeed, this suggests that control over the microstructure from poly- to nanocrystalline provides us an opportunity to exploit many of their unique physical properties and extends its utilization as an advanced nanoengineering material.

Conventionally CVD diamond uses hydrocarbon such as methane in high hydrogen dilution gas mixtures.[1] Interest becomes special when one replaces the hydrogen dilution with either noble gas and/or impurity incorporations.[2,5] There are several ways to induce nanostructuring in carbon-based materials outlined in various reports.[6–10] The potential *n*-type dopants of diamond are of particular interest which may enhance the electron field-emission properties of disordered and nanocrystalline carbon films by providing electrons close to the conduction band[4,11] and helping control the film microstructure by introducing specific types of defects.[12] *p*-type doping is also important, but it has been achieved with the

a)Author to whom correspondence should be addressed; electronic mail: sxg535f@smsu.edu

only known acceptor in diamond; boron (B).[13] However, the synthesis of diamond and diamondlike or disordered carbon thin films with *n*-type conductivity is still interrogative and is a subject of intense research.[14] A great deal of interest exists on sulfur (S) besides nitrogen and phosphorus due to the experimental and theoretical findings that it is a promising donor dopant in diamond.[15] A considerable amount of work has been performed on the nature of impurities in carbon films and some of the earlier works demonstrated the induction of shallow donor levels in diamond through the incorporation of S, but concrete experimental evidence on the potential role of sulfur as an *n*-type donor in diamond has yet to be reported.[16]

The electronic properties (band gap and density of states) are known to be sensitive to the structure or microstructure including sp^3/sp^2 C fraction, GBs or defects, and impurities usually influenced by processing conditions. The electronic density of states (DOS) of nanostructured carbon consists of two types of states: the σ bonds of sp^3 and sp^2 sites form σ states in the valence band and σ^* states in the conduction band separated by a band gap of about 5 eV. The sp^2 sites and any sp^1 sites also possess more weakly bonding π states giving rise to filled π and empty π^* states, that lie close to the Fermi level largely within the σ-σ^* gap. Therefore, π states control the optical gap and the electronic properties of disordered carbons, while the mechanical properties are governed by σ states.[17,18] In addition, the electronic structure is also largely controlled by the size of the sp^2 C clusters (chain or ring formation) than that of its absolute concentration.

There are a variety of characterization techniques investigating the electronic structure in terms of pseudogap and shape of band tails of several disordered carbon material[19] that include photoemission spectroscopy (PES),[20] electron-energy-loss spectroscopy (EELS),[21] and optical-absorption spectroscopy, to name a few.[22] While photoemission and EELS probe the filled valence-band states and empty conduction-band states, respectively, the optical absorption determines the transitions between the filled and empty states. On the other hand, scanning tunneling microscopy (STM) and scanning tunneling spectroscopy (STS) are two of the most efficient tools for investigating the electronic states within a few eV of the Fermi level. They offer another means to probe electronic structure with additional facility of detecting inhomogeneity of the surface at a spatial resolution of nanometer—a feature of particular importance when studying composite materials.[19,23] The real advantages of STS are that a single technique can measure both the filled and empty states and it is sensitive to a dopant density down to $\sim 10^{15}/\mathrm{cm}^3$ in semiconductors. In order to gain an insight on the surface characteristics crucial to the field-emission efficiency of these materials,[12] we conducted topographic and electronic properties of undoped (*n*-C) and sulfur-modified nanocrystalline carbon (*n*-C:S) films by STM/STS in ultrahigh vacuum and determined the Fermi-level shift caused due to sulfur impurity incorporation, if caused. In this work, we report our findings on the influence of sulfur addition on the electronic structure of nanocrystalline carbon films deposited using filament-assisted chemical-vapor deposition (HFCVD).

II. EXPERIMENT

Sulfur-incorporated nanocrystalline carbon (*n*-C:S) films were synthesized in a custom-built HFCVD reactor on mirror-polished 1.4-cm-diameter Mo substrates, which is described in detail elsewhere.[6] Briefly, a 2.0% CH_4:H_2 gas mixture with a total flow of 100 SCCM (standard cubic centimeter per minute) was directed through a rhenium (Re) filament heated to 2500 °C. High-purity hydrogen sulfide (H_2S) in high hydrogen dilution was used as the source of sulfur atoms (dopant) and varied between 0 and 500 ppm with 100-ppm interval. All of the films were deposited at a substrate temperature of 900 °C. The reason of selecting these growth parameters was based on our excellent electron field-emission properties from these films reported earlier.[8] The films thickness was around 1–1.5 μm as measured mechanically using a Tencor surface profilometer. The sulfur incorporations in the solid films were quantified to be ~1.2 at. %, determined by x-ray photoelectron spectroscopy (XPS) and Auger electron spectroscopy (AES) depth profiling techniques described in our earlier work.[24] For the scanning tunneling microscopy measurements, the samples were transferred into the UHV chamber (pressure below 2×10^{-10} mbars). A commercial Omicron VT-STM (UHV-STM) was used. For spatial measurements, the mechanically prepared tungsten STM tip is biased to a certain voltage and is scanned over the sample surface, and its height is controlled by interrupting the feedback to give a constant tunneling current (I) mode, which allows the topographic imaging of the sample surface. STM images were collected from a sample area of 1×1 $\mu\mathrm{m}^2$ with 100×100 raster points, and out of these 40×40 points were used for spectroscopy. Given that the STS technique is quite sensitive to both the tip and sample surface structure and nanocrystalline carbon is a form of disordered carbon, we were careful to present only those which are truly representative of the surface studied. In this respect, we have measured $I-V$ curves on a few samples and at various positions on each sample. In STS, the tip is held at a fixed height above some position on the sample and the tunneling current (I) to the tip is measured as a function of the tip or sample bias (V). Since the tunneling current depends upon the DOS of the tip and the sample, given the metallic nature of the tip (i.e., tungsten), the DOS of the tip does not influence the overall shape of the specimens' DOS. The magnitude of the tunneling current provides a measure of the local DOS. This work focuses on the tunneling spectroscopy along with the nanoscaled topology of the sulfur-modified nanocrystalline carbon films. These results are also compared to those grown without sulfur.

III. RESULTS AND DISCUSSION

Figure 1 shows the characteristic STM images of the surface for the *n*-C and *n*-C:S films in scales of 1×1 $\mu\mathrm{m}^2$, 100×100 nm^2, and 20×20 nm^2, respectively. The STM images were obtained using the bias voltage of $V=-1.0$ V ap-

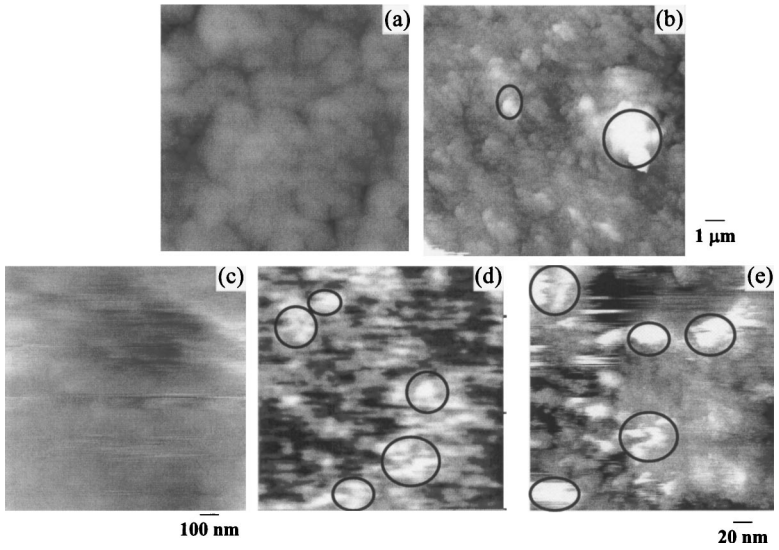

FIG. 1. High-resolution scanning tunneling microscope images of nanocrystalline carbon films without (*n*-C) (left) and with sulfur (*n*-C:S) (right) showing the topographical differences on sulfur addition in two different scales (top and bottom). The high-resolution STM images show localized regions of higher conductivity (marked by circles) of a few nanometer in diameter surrounded by less conductive regions. The scale bar is provided with the corresponding figures. Tunneling conditions: $I=1.0$ nA, $V_{tip}=-1$ V.

plied to the sample and the tunneling current of $I=1$ nA. It is evident from the STM images that the surface properties of the films depend upon the sulfur incorporation and exhibit granular structure. The surface topography also depict that the root-mean-square (rms) roughness decreases with sulfur incorporation of the order of a few angstroms. High-resolution STM images exhibit localized regions of higher conductivity (sp^2-bonded carbon) of several nanometers in diameter surrounded by less conductive (sp^3-bonded carbon) host regions, which is indeed promoted due to the sulfur incorporation in the CVD process and in the films [see Figs. 1(b), 1(d), and 1(e)]. These images reveal some of the noteworthy features:(i) the presence of both sp^3- and sp^2-bonded carbon, which is indispensable for sustainable field emission; (ii) the existence of sp^2-bonded carbon in either aggregate or dispersed state; and (iii) the clusters of hills or bumps on the film surface with different sizes imbibed in insulating matrix and forming composite mixture at nanoscale. Another evidence in support of the above-mentioned observations is based on the concept of percolation (a mix of conducting-insulating/semiconducting material—where the electrons are allowed to tunnel from one conductive cluster to another separated by insulating matrix) and demonstrated recently by means of room-temperature electrical conductivity measurements on these samples.[24] In the context of explaining the field-emission phenomena from such electrically heterogeneous composite structures, Latham's unifying theory[25] elucidated a vital role of both the filamentary structures (nanosized conducting channels embedded in a nonconducting nanostructured matrix) and spatially localized electronic states (midgap states). While the former was estimated using Raman spectroscopy in our earlier work,[8] the latter is measured using STS technique in the present study.

Figure 2 displays a series of I/V characteristics acquired from *n*-C:S films. Each curve is acquired at a constant tip-sample separation and the tip was displaced closer to the sample by 0, 1.2, 3.2, and 4.8 Å for curves (1)–(4) corresponding to tip currents of 0.01, 0.1, 1.0, and 5.0 nA, respectively, for a tip voltage of +2 V. As the tip-sample separation is reduced, the current increases by about one order of magnitude per angstrom, as apparent from Fig. 2. In general, the tunnel current between the STM tip and the sample depends upon the overlap of the wave functions of the tip and the sample. Neglecting factors such as the effect of electric fields on the surface DOS, the tunnel current is proportional to the sample DOS, the tip DOS, and the tunneling current matrix element or transmission function, which depends strongly on the tip voltage.[26] It has been demonstrated that the sample DOS is proportional to the differential conductivity, dI/dV. However, since this term still includes the voltage-dependent tunneling matrix element, the logarithmic ratio $d\log(I)/d\log(V)=(dI/dV)*(V/I)$ provides an accurate representation of the surface DOS eliminating the tunneling matrix element.[27] Nevertheless, this ratio gives singularities in the gap for the semiconductors, because $I\cong 0$ when the DOS is zero in the gap. To circumvent this problem, suggested by Feenstra and Stroscio,[28] a broadening procedure and running $I-V$ averaging were adopted when calculating logarithmic ratio. Since this broadens DOS at the band edges, we use raw dI/dV to define the band edges.

Figures 3 and 4 represent the STS spectra in terms of tunneling current (I) versus sample voltage (V), differential conductivity (dI/dV), and normalized differential conductiv-

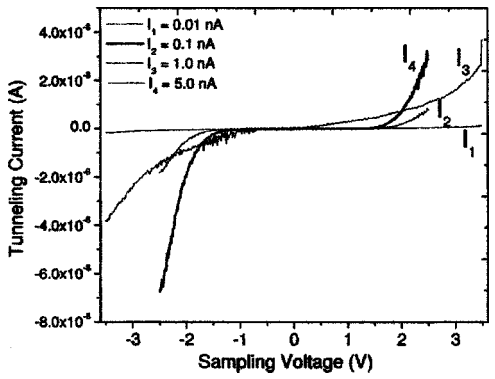

FIG. 2. Shown are the typical curves for as-deposited sulfur-incorporated nanocrystalline diamond sample taken at different tip heights. The tip heights *n*1-*n*4 correspond to tip current of $I_1=-0.1$ nA, $I_2=0.1$ nA, $I_3=1$ nA, and $I_4=5.0$ nA, at a sample voltage of +2 V.

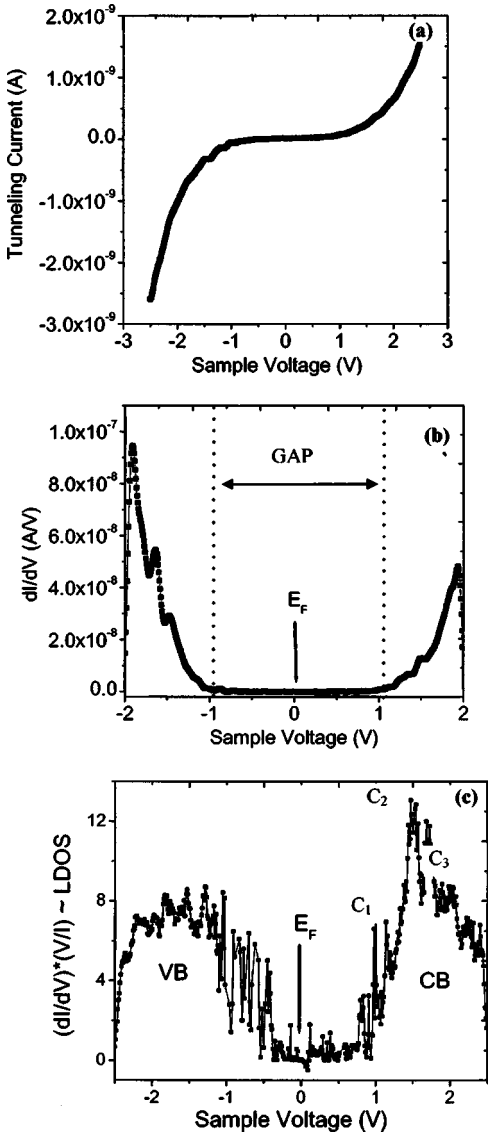

FIG. 3. Shown are (a) tunneling current (I) vs sample voltage applied (V), (b) the corresponding differential conductivity (dI/dV), and (c) the corresponding $[(dI/dV)*(V/I)] \propto$ DOS for n-C films grown by hot-filament CVD.

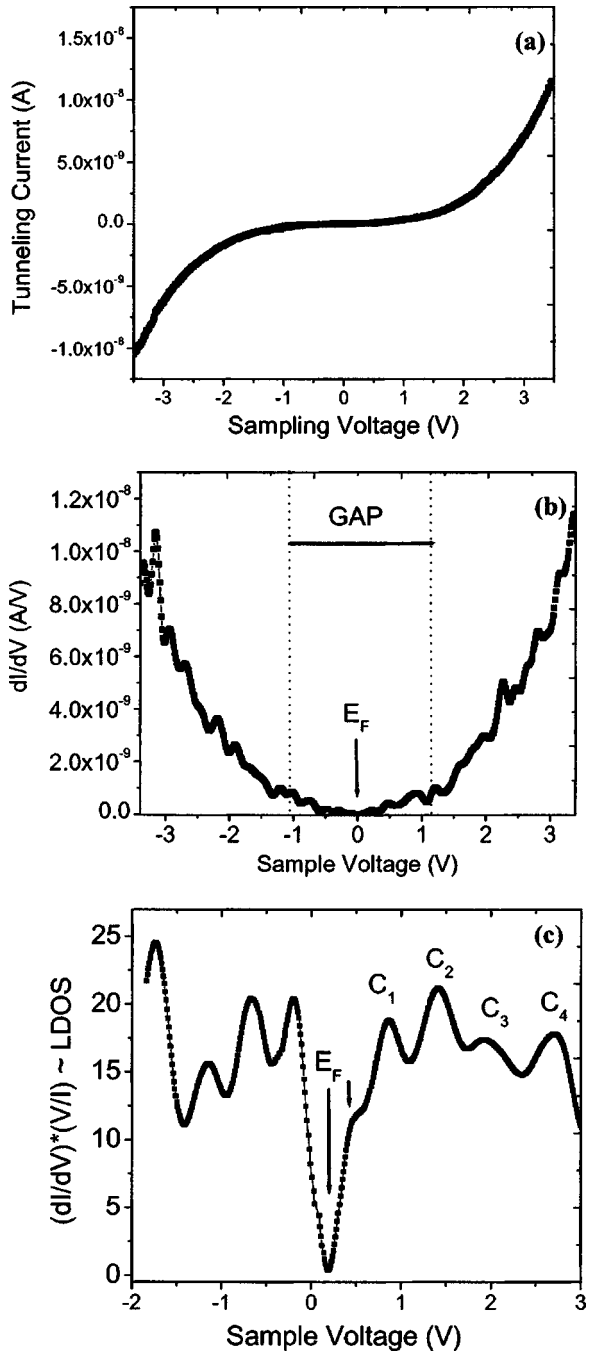

FIG. 4. Shown are (a) tunneling current (I) vs sample voltage applied (V), (b) the corresponding differential conductivity (dI/dV), and (c) the corresponding $[(dI/dV)*(V/I)] \propto$ DOS n-C:S grown by hot-filament CVD with 500 ppm of $[H_2S]$ in gas phase at $T_S = 900$ °C.

ity (dI/dV) (V/I) for the undoped (n-C) and sulfur-incorporated nanocrystalline (n-C:S) thin films, respectively. In order to have contribution specifically from the surface states, the tip height was sufficiently higher yielding in relatively larger gap in DOS as compared to that from the bulk states. $I-V$ curves also show that the tunneling current increases on sulfur incorporation, consistent with the increase in bulk conductivity [see Figs. 3(a) and 4(a)].[16] Since the conductivity of the samples is relatively high, no interference of the interface hampers the measurements. It has been observed that for the doped or impurity incorporated materials/semiconductors, tunneling current is a reasonable indication of the type of doping. The tunneling current in the positive bias is higher than that in the negative bias and vice versa. With an additional advantage of nanometer spatial resolution, STS works quite well for the determination of band gap (difference between the conduction- and valence-band edges; CB and VB, respectively) near to the Fermi level (E_F).

The band gap in the amorphous or disordered semiconductor must be defined with care and in a particular fashion, because the band states tail into the gap. We choose to adopt similar method described in Ref. 23, i.e., by defining each band edge by taking intercept of dI/dV at the valence- and conduction-band slopes in the region ±2 V away from the Fermi level to define band edges. The window energy of ±2 V was selected because this definition provides the same band gap at tip heights of $n3$ and $n4$ for the as-deposited samples. Recalling that the valence and conduction bands of the disordered carbon are formed of π states, the π bands

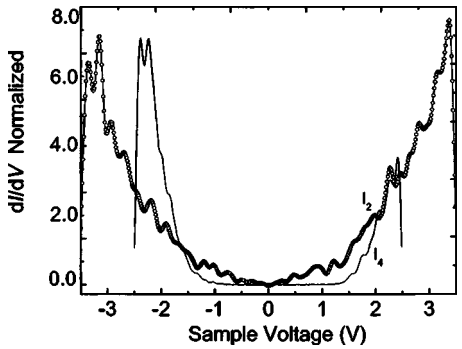

FIG. 5. Shown are the differential conductivity dI/dV, normalized to its current at 2 V for two tip heights $n2$ and $n4$ for a n-C:S sample grown with 500 ppm of $[H_2S]$ in gas phase at $T_S=900$ °C. This shows that surface layer is sp^2 C-rich (narrower gap) as compared to bulk (larger gap).

should lie symmetrically (with respect to positive and negative sample bias voltages) about midgap in simple sp^2-bonded lattices, which is much more apparent in the normalized differential conductivity plot [Figs. 3(b) and 4(b)]. The observed asymmetry of the band tails in n-C and n-C:S shows that the disorder is not simply due to the presence of different sp^2 configurations (ringlike versus chainlike), but may also be due to the distortions resulting in due to the mixing of s and p states.[29] Additionally, the slopes of the valence bands are steeper than that of the CB as it implies that disorder broadens the CB more than the VB in n-C and n-C:S. Also the E_F (0 V) is lying close to unfilled states suggesting n-type character of the n-C:S material. The dI/dV curve is much more flat for n-C than that of n-C:S [Figs. 3(b) and 4(b)]. The normalized ratio of the tunneling conductivity also shows singularities in the gap region as the tunneling current is close to zero [Fig. 3(c)] for the materials having a finite gap such as n-C. The separation of the fundamental bands (E_g) calculated from the dI/dV curves (not shown here) shows an energy gap of approximately 2.5 and 0.1 eV for n-C and n-C:S, respectively. In general, it is very useful to compare the DOS observed from STS with the data calculated from other methods. Since the resulting tunneling gap [see Fig. 5(a)] varies in a similar fashion to that measured using spectroscopic ellipsometry measurements[12] with sulfur addition, it indicates that the STS is a reliable technique for DOS for n-C:S samples. Above all, the STS spectrum of n-C [Fig. 3(c)] resembles to high-density diamondlike carbon[19] (DLC) or boron-doped tetrahedrally amorphous bonded carbon (ta-C:B; defined as a-C with high content of sp^3 C of 85%).[23]

The surface and bulk states contribution to the eventual DOS measured by scanning tunneling microscopy in spectroscopic mode STS is distinguished by measuring $I-V$ curves at different tip heights. The bulk DOS dominates the differential conductivity dI/dV spectra at lower tip heights, while the surface layer DOS contributes more to dI/dV spectra at lower tip heights. Since the current magnitude varies strongly with tip heights, dI/dV spectra must be normalized to the absolute value of the current at some arbitrary tip voltage. Figure 5 displays the normalized differential conductivity to its current at an arbitrary voltage of 2 V for two of the tip heights in order to distinguish the surface layer from bulk for one of the representative n-C:S sample grown with 500 ppm of $[H_2S]$ at 900 °C. The narrower gap of the surface layer (higher tip heights or alternatively low tunneling current; I_2) is due to its higher sp^2-bonded carbon content in contrast with the bulk (lower tip heights or alternatively higher tunneling current; I_4). The presence of an sp^2-rich surface layer has previously been inferred from *ex situ* spectroscopic ellipsometry measurements for the same samples.[30]

Figures 3(c) and 4(c) show the presence of peaks and oscillatory features in the DOS of the sp^2-bonded C-rich samples. They are reasonably reproducible for all of the samples and in all of the regions of the samples investigated. They are not dependent upon the STM system or the STM tip material (Ir–Pt used in air, W used on UHV) and they are not due to extrinsic effects such as contamination. We attribute the DOS features to graphitic bonds as explained.

The assignment of these surface DOS features in the conduction band of the Figs. 3(c) and 4(c) was carried out following notation in Ref. 31. In a recent work by Arena *et al.*,[23] states due to localized π bonding in surface DOS measured by STS were reported at 1.7, 2.8, and 3.6 eV and in the case of graphite, peaks close to these values (1.7, 2.5, and 3.5 eV) were assigned as π^* band, an extrinsic surface state and a bulk state, respectively. The present DOS features are observed at (C_1), 1.4 (C_2), 2.07 (C_3), and 2.72 (C_4) [Figs. 3(c) and 4(c)] exhibiting the graphitization of the surface layer similar to the computed ones for ta-C, and C_2 and C_4 peaks visible in STS spectra are from sp^3-rich structures. The C_1 state is assigned to be the π^* state that resembled well with the $C1s \rightarrow \pi^*$ transition in the experimental x-ray appearance near-edge spectroscopy[31] (XANES) and XPS (Ref. 12) spectra. Therefore, we suggest that the presence of a well-defined C_1 state on spectra is a clear indication of the graphitic reconstruction of the surface.

We have conducted STS measurements on sulfur-incorporated nanocrystalline diamond samples as a function of sulfur incorporation. Typical STS spectrum is shown in Fig. 4. Figure 6 shows the variation of the band gap and the position of the Fermi level from midgap. According to the STS definition, bias of 0 V corresponds to the E_F. It is clear that E_F is closer to the CB than the VB and additional DOS appears between the CB edge and the VB for n-C:S samples shown in Fig. 6(b). We suggest that this may be due to the donor state occurring due to S addition during the CVD growth or incorporated in solid thin films. Alternatively, sulfur is causing n-type doping in n-C with increasing $[H_2S]$. In fact, similar proposition has been reported previously, where temperature-dependent field emission was employed to demonstrate this phenomenon.[24] The band gap begins to close up as the sulfur concentration in gas phase ($[H_2S]$) is raised above 200 ppm. This closing or reduction in the band gap is due to the carbon reverting to more sp^2 bonding at higher S content [see Fig. 6(a)]. This effect was seen previously in spectroscopic ellipsometry measurements of the gap [Fig. 6(a)].[24] Notice that the Fermi level remains above midgap even when the gap closes.

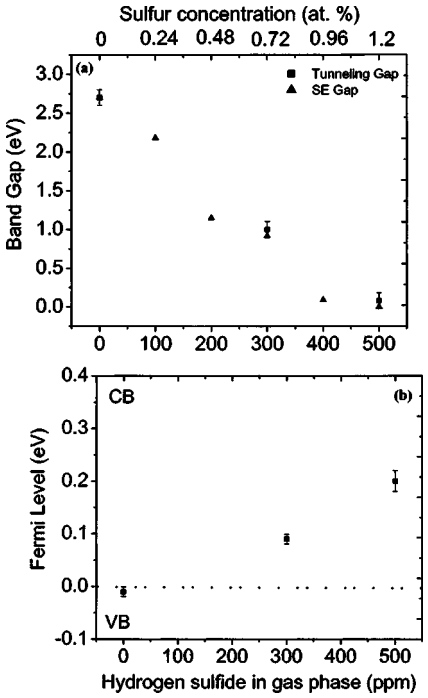

FIG. 6. Variation of (a) band gaps and (b) Fermi-level energy of nanocrystalline carbon films plotted as a function of hydrogen sulfide concentration in gas phase, i.e., during deposition. Corresponding atomic fraction of sulfur in solid films is also provided (top abscissa). The maximum value of band gap corresponds to maximum sp^3 C content. The band gap determined using spectroscopic ellipsometry modeling is also shown for comparison.

IV. CONCLUSIONS

In conclusion, we elucidated a correlation between the microstructure (including grain size, topology, and chemical bonding) and electronic structure of the surface of sulfur-incorporated nanocrystalline diamond thin films by scanning tunneling microscopy and scanning tunneling spectroscopy. Along with a systematic decrease in grain size and surface roughness with increasing hydrogen sulfide concentration in the gas phase (S/C ratio from 0.00 to 0.162), there is a modification in the electronic structure. Alteration due to the sulfur addition not only results in the introduction of spatially localized defect states, but also in partial doping. For instance, the Fermi level is found to shift towards the conduction band in the sulfur-incorporated samples, indicating that *n*-type doping occurs. This *n*-type doping is possibly occurring due to incomplete ionization of S atoms demonstrated using scanning tunneling microscopy in spectroscopy mode. This synthesis-specific nanocomposite material (highly conductive sp^2 C regions surrounded by less conductive sp^3 C regions in an aggregate or dispersed state) has a strong potential as cold cathode or field emitters, as low-temperature thermionic emitters, and thermionic power generators.

ACKNOWLEDGMENTS

This research work is supported by the Department of Energy (Grant No. DE-FG02-01ER45868). We gratefully acknowledge the use of UHV-STM facilities at the University of Cambridge, UK (Dr. C. Durkan) and North Carolina State University, Raleigh (Dr. R. J. Nemanich and Joe Tedesco) in the execution of this work.

[1] D. M. Gruen, Annu. Rev. Mater. Sci. **29**, 211 (1999), and references therein.
[2] J. Robertson, Surf. Coat. Technol. **50**, 185 (1992).
[3] J. Robertson, Tribol. Int. **36**, 405 (2003).
[4] S. Bhattacharyya *et al.*, Appl. Phys. Lett. **79**, 1441 (2001).
[5] R. Haubner, S. Bohr, and B. Lux, Diamond Relat. Mater. **8**, 171 (1999).
[6] S. Gupta, B. L. Weiss, B. R. Weiner, and G. Morell, J. Appl. Phys. **89**, 5671 (2001).
[7] S. Gupta, B. L. Weiss, B. R. Weiner, and G. Morell, Appl. Phys. Lett. **79**, 3446 (2001), and references therein.
[8] S. Gupta, B. R. Weiner, and G. Morell, J. Appl. Phys. **91**, 10 088 (2002).
[9] T. D. Corrigan, A. R. Krauss, D. M. Grüen, O. Auciello, and R. P. H. Chang, Mater. Res. Soc. Symp. Proc. **593**, 233 (2000).
[10] J. Robertson, J. Vac. Sci. Technol. B **17**, 659 (1999); A. Illie, A. C. Ferrari, T. Yagi, and J. Robertson, Appl. Phys. Lett. **76**, 2627 (2000).
[11] S. Bhattacharyya, K. Walzer, H. Hietschold, and F. Richter, J. Appl. Phys. **89**, 1619 (2001).
[12] S. Gupta, B. R. Weiner, and G. Morell, J. Appl. Phys. **92**, 5457 (2002).
[13] M. Werner, R. Job, A. Zaitsev, W. R. Fahrner, W. Seifert, C. Johnston, and P. R. Chalker, Phys. Status Solidi A **154**, 385 (1996).
[14] R. Kalish, A. Reznik, C. Uzan-Saguy, and C. Cytermann, Appl. Phys. Lett. **76**, 757 (2000).
[15] T. Miyazaki and H. Okushi, Diamond Relat. Mater. **10**, 449 (2001), and references therein.
[16] S. Gupta, A. Martinez, B. R. Weiner, and G. Morell, Appl. Phys. Lett. **80**, 1471 (2002).
[17] J. Robertson and E. P. O'Reily, Phys. Rev. B **35**, 2946 (1987).
[18] G. Fanchini, S. C. Ray, and A. Tagliaferro, Diamond Relat. Mater. **12**, 891 (2003).
[19] V. I. Ivanov-Omskii *et al.*, Pis'ma Zh. Tekh. Fiz. **24**, 28 (1998).
[20] J. Schafer *et al.*, Phys. Rev. B **53**, 7762 (1996).
[21] M. Chhowalla, J. Robertson, C. W. Chen, S. R. P. Silva, C. A. Davis, G. A. J. Amaratunga, and W. I. Milne, J. Appl. Phys. **81**, 139 (1997).
[22] F. Xiong, Y. Y. Wang, and R. P. H. Chang, Phys. Rev. B **48**, 80 106 (1993).
[23] C. Arena, B. Kleinsorge, J. Robertson, W. I. Milne, and M. E. Welland, J. Appl. Phys. **85**, 1609 (1999).
[24] S. Gupta, B. R. Weiner, and G. Morell, J. Appl. Phys. **95**, 8314 (2004), and references therein.
[25] R. G. Forbes, Solid-State Electron. **45**, 779 (2001), and references therein.
[26] R. M. Feenstra, J. A. Stroscio, and A. P. Fein, Surf. Sci. **181**, 295 (1987); P. Martensson and R. M. Feenstra, Phys. Rev. B **39**, 7744 (1989).
[27] J. A. Stroscio and R. M. Feenstra, in *Scanning Tunneling Microscopy*, edited by J. A. Stroscio and W. J. Kaiser (Academic, New York, 1993), p. 139–140; R. M. Feenstra, Phys. Rev. B **50**, 4561 (1994).
[28] R. M. Feenstra and J. A. Stroscio, J. Vac. Sci. Technol. B **5**, 923 (1987).
[29] J. Robertson, Philos. Mag. B **76**, 335 (1997).
[30] S. Gupta, B. R. Weiner, and G. Morell, Thin Solid Films **455–456**, 422 (2004).
[31] K. J. Koivusaari, T. T. Rantala, J. Levoska, and S. Leppävuori, Appl. Phys. Lett. **76**, 2794 (2000).